https://doi.org/10.1007/s41230-019-9014-9

Effect of Ca addition on solidification microstructure of hypoeutectic Al-Si casting alloys

Xiang-yi Jiao[1], Chao-feng Liu[1], Jun Wang[1], Zhi-peng Guo[1,2], Jun-you Wang[3], Zhuo-ming Wang[3], Jun-ming Gao[3], *Shou-mei Xiong[1,2]

1. School of Materials Science and Engineering, Tsinghua University, Beijing 100084, China

2. Key Laboratory for Advanced Materials Processing Technology, Tsinghua University, Beijing 100084, China

3. Hong Bang Die Casting (Nantong) Co., Ltd., Nantong, China

Abstract: The effect of Ca addition on the solidification microstructure of hypoeutectic Al-Si casting alloys was investigated using scanning electron microscopy (SEM) and differential scanning calorimetry (DSC) methods with particular attention focused on the change of morphologies of primary α-Al and eutectic silicon. Meanwhile, solute distribution in solid-liquid was simulated according to Scheil-Gulliver law. Results showed that primary α-Al and eutectic silicon were refined as Ca content increased because of the variation of the solute concentration in liquid. The addition of Ca increased the nucleation sites like Al_3Ti or Al_2Cu to promote the nucleation of primary α-Al. Affected by modification effect of Ca, the shape of eutectic silicon changed from flake to fibrous structure. In addition, coarse plate Ca-rich phases could be found along the grain boundary with high Ca content.

Key words: Ca addition; primary α-Al; eutectic silicon; refinement

CLC numbers: TG146.21 **Document code:** A **Article ID:** 1672-6421(2019)03-153-08

Due to their high strength, light weight and excellent casting properties, hypoeutectic Al-Si casting alloys are widely applied in automotive parts like the automobile hub, steering wheel and dash board [1-8]. The microstructure of hypoeutectic Al-Si alloys comprised primary α-Al, eutectic silicon and intermetallic compound [9]. Refining and regulating these microstructures becomes an important way to improve the mechanical properties and the casting quality [10].

Microalloying elements such as Ti, B, and Sr usually serving as grain refiner or modifier are added to improve alloy properties. The Al-Ti-B master alloys are effective nucleating agents for Al-Si alloys. By adding Al-5Ti-B master alloys, Riestra et al.[11] found that the Al_3Ti and TiB_2 particles were formed and primary α-Al was refined. After adding 0.15wt.% B, Wu et al.[12] found that α-Al dendrites were significantly refined. Numerous AlB_2 particles formed prior to the α-Al grains in the melts increased the heterogeneous nucleation sites. As for eutectic silicon, it is a common understanding that the impurity induced a twinning effect [13, 14]. Li et al.[15] discovered that Sr atoms segregated at the intersection of Si twins inducing multiple twinning growth. In addition, Timpel et al.[16] found Sr-segregations were more extended structures restricting the growth of eutectic Si and changing its morphology.

Similar with Ti, B and Sr, Ca element can also act as grain refiner or modifier in hypoeutectic Al-Si alloys. Based on thermal analysis, Kumariet al.[17] found Ca decreased the eutectic temperature and changed the shape of eutectic Si from acicular to fibrous. Using EPMA and EBSD analysis, Zaldívar et al.[18] observed a plate-like calcium-rich phase, i.e., hexagonal Al_2Si_2Ca with space group P-3 m1 (164), a=0.413 nm, c=0.7145 nm. Ludwig et al.[19] did not find a flake-to-fibrous transition even if Ca additions were 300 ppm.

However, unlike other microalloying elements, microstructure modification of hypoeutectic Al-Si alloy by Ca was not clear. In this study, the effect of Ca addition on the microstructure of hypoeutectic Al-Si casting alloys was investigated by employing OM, SEM and DSC. Particular focus was on the effect of Ca addition on the evolution of microstructure and solute distribution during solidification.

1 Experimental procedure

In this work, a commercial hypoeutectic alloy

***Shou-mei Xiong**

Male, Ph.D., Professor. Research interests: Al and Mg alloy high pressure die casting and microstructure simulation during solidification.

E-mail: smxiong@tsinghua.edu.cn

Received: 2019-01-21; Accepted: 2019-03-13

AlSi10MnMg was used, and its chemical composition is listed in Table 1. The alloy was melted in a graphite crucible at 720 °C, and was held for 30 min to avoid potential solute segregation. The element Ca was then added in the form of Al-10wt.% Ca. The nominal addition levels were 0wt.%, 0.02wt.%, 0.1wt.%, and 0.5wt.%. The melt was stirred for 30 s and then kept at 720 °C for 30 min, and finally poured into a preheated permanent H13 mold with a cooling rate of 20 °C·s^{-1}. The casting was a Φ15 mm × 100 mm cylindrical bar. Samples for SEM (5 mm × 5 mm × 10 mm), DSC (5 mm × 5 mm × 1 mm), CT (Φ1 mm × 10 mm) and tensile test bar (Φ10 mm × 90 mm) were extracted along the centerline of the casting using a wire-electrode cutting method.

The metallographic samples were mounted by epoxy resin, ground on SiC papers (#400, #800, #1200, #1500 and #2000) and polished with ethyl alcohol based colloidal silica suspension (2.5, 1 and 0.5 μm). After ultrasound cleaning, the microstructure was observed using an optical microscope (OM). Image-Pro Plus 6.0 software was used to identify the secondary dendrite arm spacing (SDAS). For SEM observation, the samples were etched for 30 s with 0.5 vol% HF. The phase transition temperature was obtained by the Differential Scanning Calorimetry (DSC, NETZSCH STA 449F3) with a cooling rate of 10 °C·min^{-1} from 800 °C to 400 °C. To further understand the effect of Ca addition on solute distribution, JMatPro® software was used to simulate the solute change in liquid during solidification.

Table 1: Chemical composition of AlSi10MnMg hypoeutectic Al-Si alloy (wt.%)

Si	Fe	Cu	Mn	Mg	Zn	V	Ti	Sr	Al
9.5–11.5	<0.15	<0.03	0.5–0.8	0.1–0.5	< 0.07	<0.07	0.04–0.15	0.01–0.025	Bal.

Tensile tests were performed on a WDW electronic universal testing machine with a loading rate of 1 mm·min^{-1}. All tests were performed at ambient temperature. After tensile testing, the fracture location was sampled to analyze the fracture morphology with different Ca additions.

2 Results

2.1 Microstructure

Figures 1(a–d) show the optical micrograph of AlSi10MnMg with different Ca contents from 0 to 0.5 wt.%. It is clear that the microstructure comprises primary α-Al and eutectic. Primary α-Al existed in a form of dendrite and globular. As Ca increased from 0wt.% to 0.5wt.%, the primary α-Al grains became smaller while eutectic remained unchanged, and when the Ca content reached 0.5wt.%, coarse plate-shaped Ca-rich phases appeared. To further analyze the effect of Ca addition on the size and shape of primary α-Al, the secondary dendrite arm spacing (SDAS) and grain size in different alloys were measured using Image-Pro Plus 6.0 software. The SDAS could be estimated by [20-22]:

$$\mathrm{SDAS} = \frac{L}{n} \tag{1}$$

where L is the length of the straight line drawn from one secondary dendrite arm to another; n is the number of secondary dendrite arm passed by the line. Three different straight lines were used in the same sample to ensure the accuracy of experiment results. The grain size (D) could be expressed by Eq. (2) [23, 24]:

$$D = 2\sqrt{\frac{A}{\pi}} \tag{2}$$

where A is the average area of primary α-Al grains.

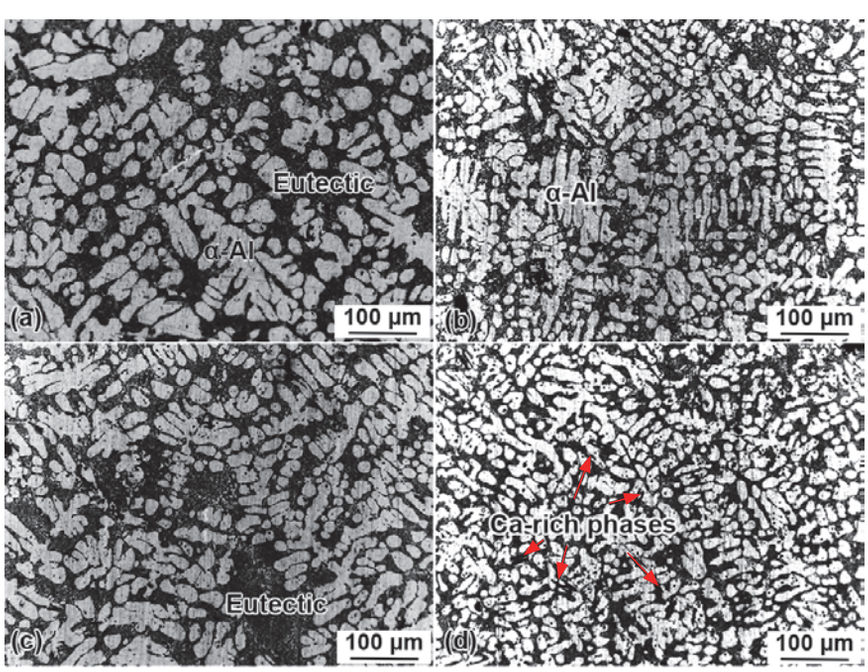

Fig. 1: Optical micrograph of AlSi10MnMg with 0wt.% Ca (a), 0.02wt.% Ca (b), 0.1wt.% Ca (c) and 0.5wt.% Ca (d)

Figures 2(a–d) show the SEM observation of the microstructure of AlSi10MnMg with 0, 0.02, 0.1 and 0.5wt.% Ca, respectively. The microstructure comprised of α-Al, eutectic and acicular Fe-rich phases. In Fig. 2(d), coarse Ca-rich phases existed along the α-Al grain boundary. Fine Al_3Ti particles were present in the inner grain. From Figs. 2(a) and (b), it can be seen that the size of eutectic Si particles did not change while the shape changed from plate to fibrous. After adding 0.1wt.% or 0.5wt.% Ca, the size of eutectic Si particles decreased significantly and more particles exhibited a fibrous shape.

Figure 3(a) shows the results of SDAS and grain size in AlSi10MnMg with different Ca levels. Both the SDAS and grain size decreased as Ca content increased. Without Ca addition, the average of SDAS was 24.8 μm. After adding 0.02wt.% Ca, the average SDAS decreased to 16.9 μm, and the average SDAS reached the lowest value of 13.7 μm when 0.1wt.% Ca was

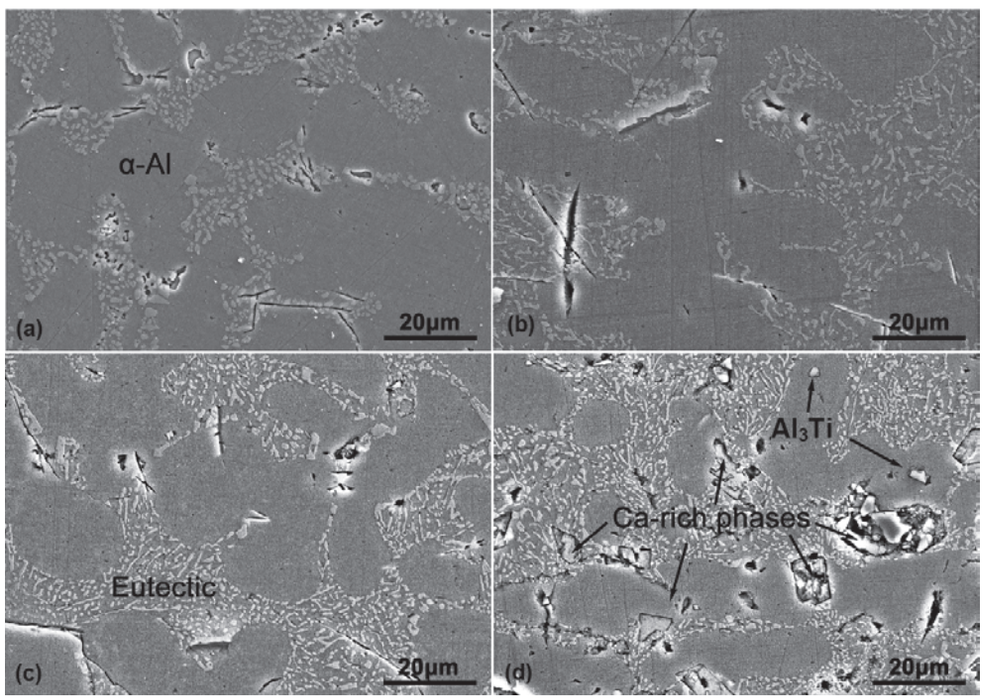

Fig. 2: SEM microstructure of AlSi10MnMg with 0wt.% Ca (a), 0.02wt.% Ca (b), 0.1wt.% Ca (c) and 0.5 wt.% Ca (d)

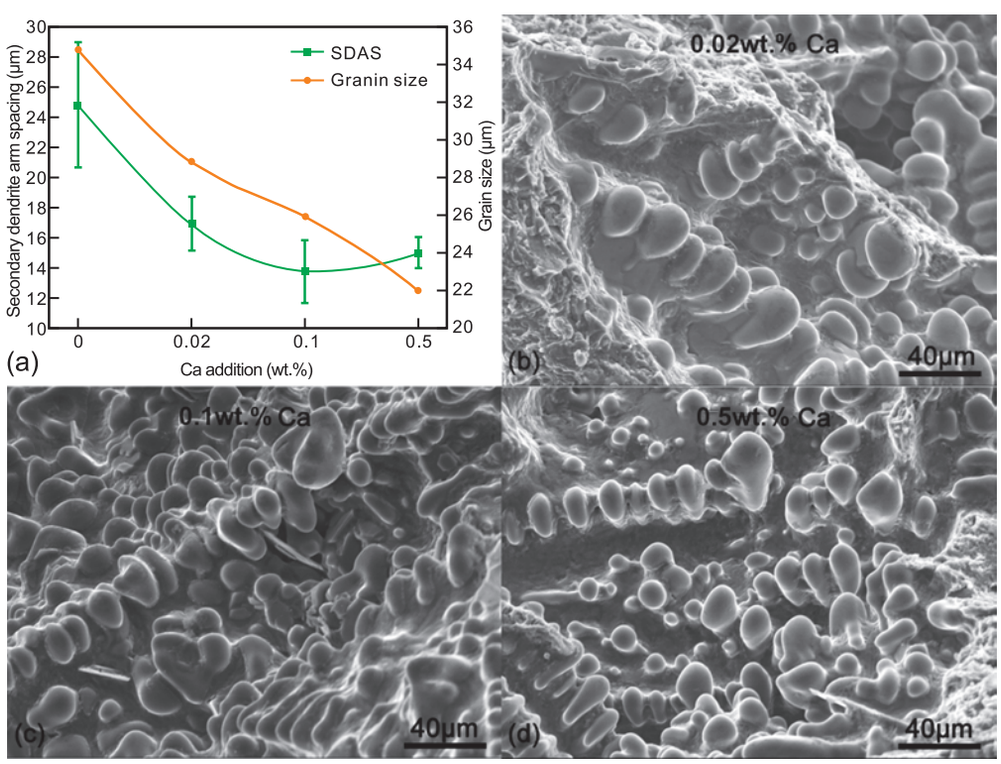

Fig. 3: (a) Secondary dendrite arm spacing and grain size in $AlSi_{10}MnMg$ with different Ca contents; 3D dendrite morphology of AlSi10MnMg with (b) 0.02wt.%Ca, (c) 0.1wt.% Ca and (d) 0.5wt.% Ca extracted from shrinkage region after fracture

employed. As Ca further increased, the average SDAS increased to 15 μm. In addition, the grain size of AlSi10MnMg without Ca addition was 34.8 μm. After adding 0.02wt.% Ca, the grain size decreased rapidly to 28.9 μm. As Ca content further increased to 0.1wt.%, the grain size of α-Al decreased to 25.9 μm. When Ca content in AlSi10MnMg was 0.5wt.%, fine dendrites with a size of 22.0 μm were present.

Figures 3(b–d) show the 3D dendrite morphology of AlSi10MnMg with 0.02, 0.1 and 0.5 wt.% Ca, respectively. The 3D dendrite microstructure was extracted from an area close to shrinkage. It is clear that the size of dendrite decreased with the addition of Ca. When Ca content reached 0.5wt.%, the growth of dendrite was restricted and the secondary dendrite arm was refined.

2.2 Solidification thermodynamics

Figure 4 shows the DSC solidification exotherms of AlSi10MnMg with different Ca levels. There are two exothermic peaks in each curve. Between 550 °C and 600 °C, the latent heat was released due to the nucleation of primary α-Al. Between 500 °C and 550 °C, the latent heat was released due to the nucleation of eutectic. Comparing with primary α-Al, solidification of eutectic would release more latent heat. To further analyze the effect of Ca addition on the phase transformation of AlSi10MnMg, a local enlarged DSC diagram is shown in Fig. 4(b). The precipitation temperature of primary α-Al in AlSi10MnMg was 581 °C. An addition of 0.5wt.% Ca raised the nucleation temperature (~1.5 °C) of primary α-Al. Meanwhile, the nucleation temperature of eutectic also rose from 557.5 °C to 561 °C. However, 0.02wt.% Ca addition would not affect the nucleation temperature of primary α-Al and eutectic.

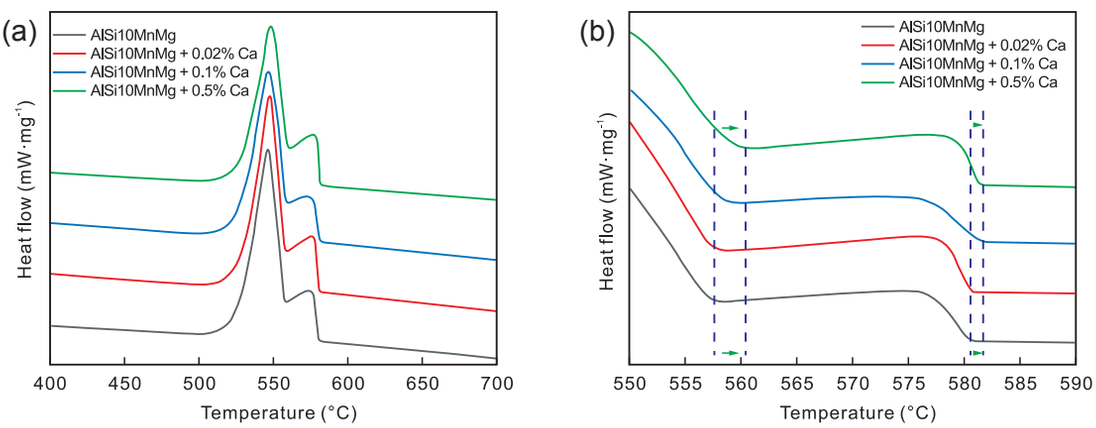

Fig. 4: Differential scanning calorimetry solidification exotherms of AlSi10MnMg with different Ca levels: (a) from 400 °C to 700 °C; (b) from 550 °C to 590 °C

3 Discussions

3.1 Refinement of primary α-Al

Figure 5 shows the morphology of the second phase particles in AlSi10MnMg with 0.5wt.% Ca. It is clear that both Ca-rich phases and Al_3Ti exist in the microstructure. In particular, coarse plate Ca-rich phases existed along the α-Al grain boundaries, in which the Ca content was 13.4wt.% (Fig. 5c). The Al_3Ti phase existed in the inner grain with a size < 5 μm. It is well-known that the Al_3Ti phase served as heterogeneous nucleation sites to promote α-Al nucleation. Employing the first-principle density functional method, Li et al.[25] found it was easier for Al(111) to nucleate on Al_3Ti (112) due to epitaxial coherency and stronger adhesion. Nayak et al.[26] believed stable reinforcement phases like Al_3Ti, Al_3Ni, Al_3Fe and Al_3Zr had good interfacial bonding with Al matrix. Gupta et al.[27] found the Al_3Ti particles generated in the melt promoted heterogeneous nucleation and had significant grain refinement effect. In addition, because of a higher melting point (~1,623 K), Al_3Ti was stable at lower temperatures. Accordingly, 0.5wt.% Ca promoted the precipitation of Al_3Ti from α-Al matrix, while Ca-rich phases and Al_3Ti were not discovered in other cases (Fig. 2). Furthermore, in Fig. 4(b), the precipitation temperature of primary α-Al phase increased with increasing Ca content which indicated more heterogeneous nucleation sites formed induced by Ca addition. To further analyze the precipitation of Al_3Ti during solidification, the precipitation of Ti was simulated using JMatPro® software based on Scheil-Gulliver theory:

$$C_L = C_0 (1 - f_s)^{(k_0 - 1)} \quad (3)$$

where C_L is the concentration of solute in liquid, f_s is the solid fraction, C_0 is the actual solute concentration (C_0=0.15%), k_0 is solute partition coefficient and dependent on the ratio between C_L and C_S. In Eq. (3), the relationship between f_s and Ti content in liquid (C_L^{Ti}) is shown in Figs. 6(a) and (b).

Figure 6(a) shows the change of C_L^{Ti} during solidification of AlSi10MnMg with different Ca additions. In the early stage of solidification, solute could not diffuse effectively in the primary α-Al because of high cooling speed. Solute was expelled and enriched in liquid. Addition of Ca promoted precipitation of Ti. However, when f_s reached 0.02%, high Ti concentration in liquid resulted in the formation of stable Al_3Ti, leading to a rapid decrease of Ti content in liquid. The surface of Al_3Ti worked as nucleation site, which increased nucleation rate. Figure 6(b) shows that AlSi10MnMg with

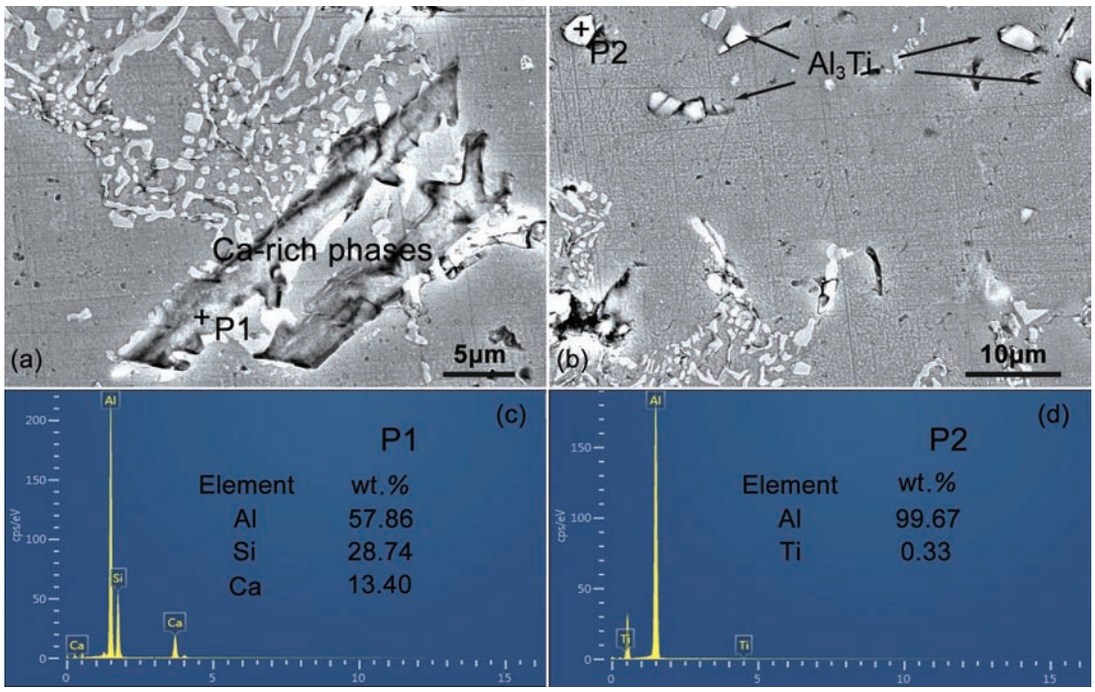

Fig. 5: Morphology of Ca-rich phases (a) and Al_3Ti in AlSi10MnMg with 0.5 wt.%Ca (b), EDS results of Ca-rich phases (c) and (d) Al_3Ti

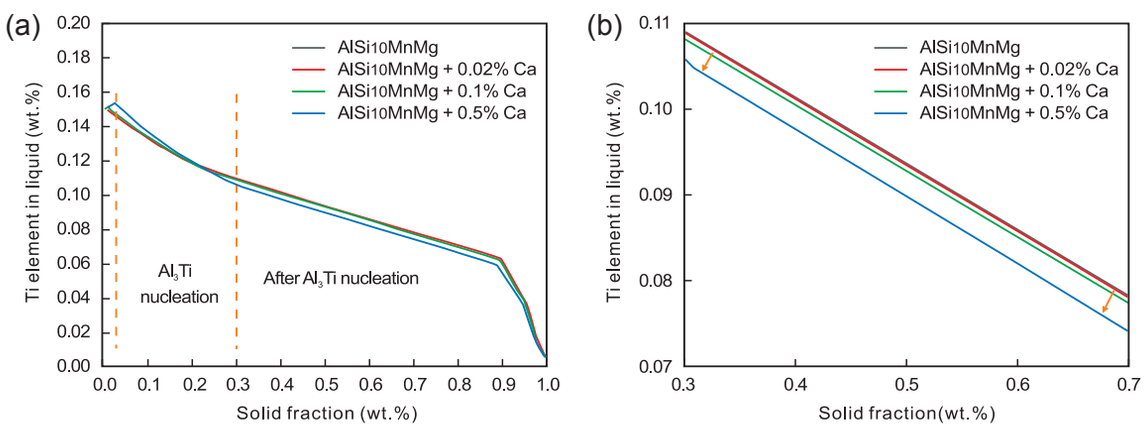

Fig. 6: Change of Ti content in liquid with increase of solid fraction simulated by JMatPro® and enlarged figure with a solid fraction from 0.3% to 0.7%

0.5wt.% Ca addition had the lowest Ti content in liquid. However, the slope of the four straight lines was the same, indicating that Ca element would not affect the solute diffusion after Al_3Ti formed. When f_s reached 0.9%, Ti content in liquid rapidly decreased. Meanwhile, the eutectic began to nucleate and exclude solute at the phase interface.

3.2 Modification of eutectic

The Sr element is added in AlSi10MnMg alloy as modifier. Figure 7(a) shows the change of Sr content in liquid during solidification. It is clear that Sr element disappeared in liquid at the beginning of solidification when 0.1wt.% or 0.5wt.% Ca was added. According to the phase diagram, Ca and Sr would form solid solution due to the similar chemical property. Figure 7(b) shows the local solid fraction between 0.3% and 0.7%. Without Ca addition, Sr exhibited a high mass fraction (~0.005%) in liquid. When high Ca content was added, Sr content was near 0% in liquid. Because eutectic solidified at the last stage, Sr would barely modify eutectic Si particles in AlSi10MnMg with high Ca content. However, from Fig. 1, it can be seen that Si particles were refined even if Sr content was low in the last solidified stage. In other words, Ca would replace Sr to refine eutectic Si particles. Similar as Sr, Ca combined with Al and Si to form coarse hexagonal Al_2Si_2Ca distributed in Si phase interface [18]. To further analyze the effect of Ca addition on eutectic Si, $AlSi_9Cu_3$ alloy (9wt.% Si, 3wt.% Cu) was used without Sr content.

Figures 8(a) and (b) show DSC solidification exotherms of $AlSi_9Cu_3$ with different Ca contents. It is clear that three exothermic peaks existed in each curve. Compared with $AlSi_{10}MnMg$, one more exothermic peak existed near 500 °C (Fig. 8a), and the related latent heat was released due to the nucleation of Cu-rich phases. Similar as $AlSi_{10}MnMg$, the nucleation temperature of primary α-Al was raised with Ca addition. It raised about 6 °C when the addition of Ca was 0.5wt.%. Like Al_3Ti, the introduction of Ca induced the

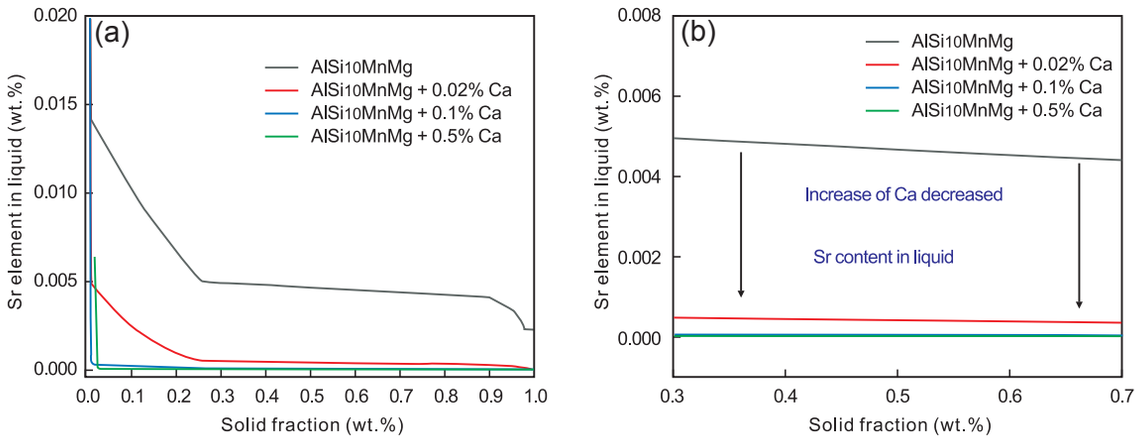

Fig. 7: Change of Sr content in liquid with increase of solid fraction simulated by JMatPro® and enlarged figure with a solid fraction from 0.3% to 0.7%

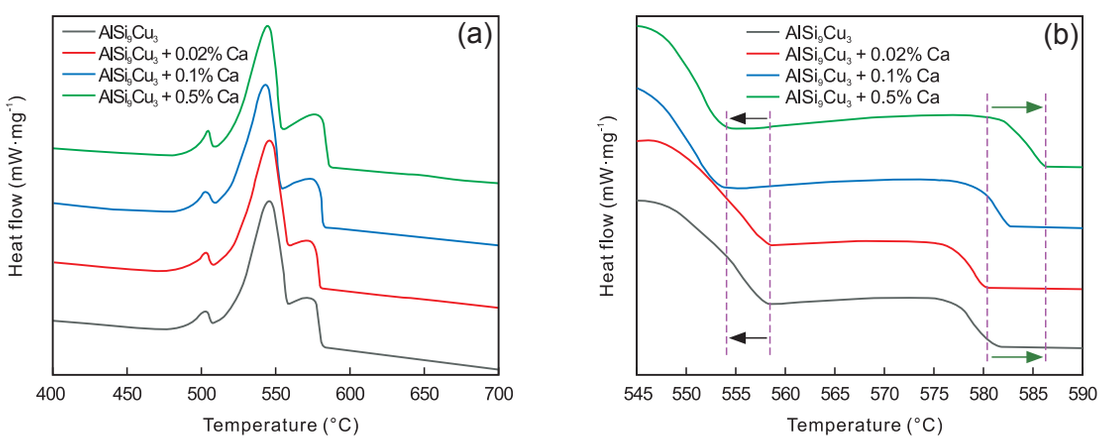

Fig. 8: DSC exotherm of $AlSi_9Cu_3$ (without Sr) with different Ca contents

formation of Al_2Cu in inner grain, which increased nucleation sites and promoted the precipitation of primary α-Al. Wang et al.[28] investigated that the crystallographic orientation relationships between α-Al and Al_2Cu was {211}Al_2Cu||{111} Al and <120>Al_2Cu||<110>Al. This indicated the formation of Al_2Cu provided driving force for α-Al nucleation[29].

However, different from the nucleation effect of Ti element, most Cu element was expelled to the solid-liquid interface, inhibiting the further growth of primary α-Al. Figures 9(a) and (b) show the Cu content in liquid under solidification. It is clear that the concentration of Cu element increased exponentially with the solid fraction [Fig. 9(a)]. Cu element was expelled and enriched in liquid. Figure 9(b) shows the local enlarged figure with a solid fraction between 0.48 and 0.52. It is clear that Ca addition further raised the concentration of Cu element in liquid. Accordingly, greater segregation formed in grain boundary restricted the growth of primary α-Al.

According to Fig. 8(b), the nucleation temperature of eutectic in $AlSi_9Cu_3$ with 0.5wt.% Ca dropped by 5 °C. The restriction of α-Al growth would further affect the precipitation of eutectic. It was found that Cu-rich phases hindered the growth of the aluminum dendrite which further restricted the precipitation

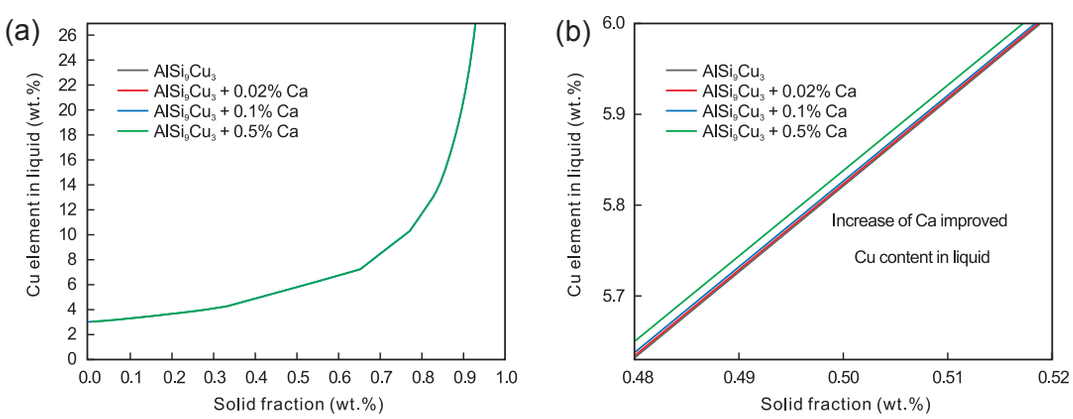

Fig. 9: Simulation result of Cu content in liquid using JMatPro®

of Si [30, 31]. In addition, decrease of nucleation temperature indicated that the eutectic grew at a lower temperature and accordingly, the refinement of eutectic Si was achieved.

Figure 10 shows the microstructure of $AlSi_9Cu_3$ with different Ca contents. It is clear that coarse flake eutectic silicon existed (Fig. 10a). As Ca addition increased, coarse flake eutectic silicon was fragmented into smaller flakes. As the Ca element further increased to 0.5wt.% in $AlSi_9Cu_3$, the shape of eutectic silicon changed into fibrous structure (Fig. 10d). In addition, coarse plate Ca-rich phases and Cu-rich phases distributed along grain boundaries..

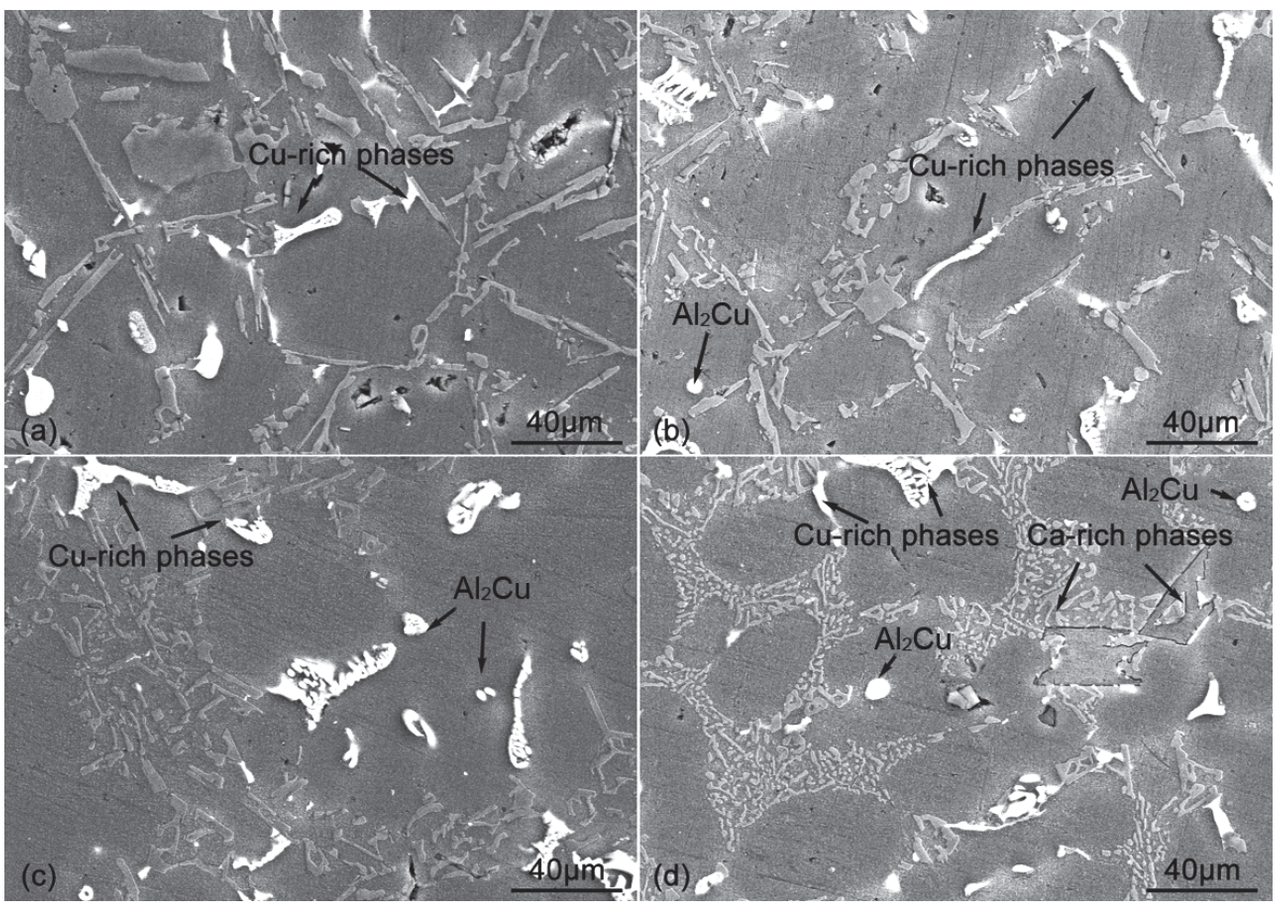

Fig. 10: SEM observation of microstructure of $AlSi_9Cu_3$ with different contents of Ca: (a) 0wt.%, (b) 0.02wt.%, (c) 0.1wt.% and (d) 0.5wt.%

The addition of Ca element in AlSi10MnMg alloy induced the formation of Al_3Ti, which increased the nucleation sites for primary α-Al. Therefore, the precipitation temperature of primary α-Al increased. Affected by early precipitation of α-Al, the effective nucleation of eutectic Si was also promoted. For $AlSi_9Cu_3$, the addition of Ca element caused Al_2Cu in α-Al grains, promoting the precipitation of primary α-Al. Meanwhile, greater solute segregation in front of the solid-liquid interface restricted the further growth of α-Al. However, different from $AlSi_{10}MnMg$, the precipitation of eutectic was also inhibited, which was related to the limitation of α-Al growth. Although the effect of Ca addition on the nucleation temperature of eutectic was different for the two hypoeutectic alloys, all eutectic Si was refined. Coarse flake shape transformed to fibrous structure with the increase of Ca, leading to the refinement of eutectic Si.

4 Conclusions

In this work, the effect of Ca addition on the solidification microstructure of hypoeutectic Al-Si casting alloys was investigated. Particular attention was focused on the change of solute during solidification. Based on the experimental data and simulation results, the following conclusions can be drawn:

(1) The increase of Ca content decreases the grain size of primary α-Al and secondary dendrite arm spacing. The eutectic Si morphology also changes from coarse flake shape to fine fibrous structure. When Ca content reaches 0.5wt.%, coarse plate Ca-rich phases can be found along grain boundaries.

(2) The addition of Ca element increases the nucleation temperature of primary α-Al by inducing the formation of heterogeneous nucleation sites like Al_3Ti or Al_2Cu. Therefore, primary α-Al is refined with the increase of Ca content. Eutectic Si morphology is also refined, affected by the modification effect of Ca.

(3) According to Scheil-Gulliver theory, addition of Ca element altered the solute concentration in liquid. This affected the nucleation temperature of primary α-Al and eutectic Si.

References

[1] Aguilera-Luna I, Castro-Román M J, Escobedo-Bocardo J C, et al. Effect of cooling rate and Mg content on the Al-Si eutectic for Al-Si-Cu-Mg alloys. Materials Characterization, 2014, 95: 211–218.
[2] Wu Y, Liao H, Yang J, et al. Effect of Si Content on Dynamic Recrystallization of Al-Si-Mg Alloys During Hot Extrusion. Journal of Materials Science & Technology, 2014, 30: 1271–1277.
[3] Guo F, Wang W, Yu W, et al. Enhanced nucleation and refinement of eutectic Si by high number-density nano-particles in Al-10Si-0.5Sb alloys. Mater. Des., 2017, 117: 382–389.
[4] Gao T, Li Z, Zhang Y, et al. Evolution of Fe-rich phases in Mg melt and a novel method for separating Al and Fe from Al-Si-Fe alloys. Mater. Des., 2017, 134: 71–80.
[5] Vlach M, Čížek J, Smola B, et al. Heat treatment and age hardening of Al-Si-Mg-Mn commercial alloy with addition of Sc and Zr. Materials Characterization, 2017, 129: 1–8.
[6] Huang H, Dong Y, Xing Y, et al. Low cycle fatigue behaviour at 300 °C and microstructure of Al-Si-Mg casting alloys with Zr and Hf additions. Journal of Alloys and Compounds, 2018, 765: 1253–1262.
[7] Wang K, Jiang H Y, Wang Q D, et al. Nanoparticle-induced nucleation of eutectic silicon in hypoeutectic Al-Si alloy. Materials Characterization, 2016, 117: 41–46.
[8] Das P, Samanta S K, Chattopadhyay H, et al. Effect of pouring temperature on cooling slope casting of semi-solid Al-Si-Mg alloy. Acta Metallurgica Sinica (English Letters), 2012 25: 329–339.
[9] Mao F, Yan G, Li J, et al. The interaction between Eu and P in high purity Al-7Si alloys. Materials Characterization, 2016, 120: 129–142.
[10] Cho Y H, Lee H C, Oh K H, et al. Effect of Strontium and Phosphorus on Eutectic Al-Si Nucleation and Formation of β-Al5FeSi in Hypoeutectic Al-Si Foundry Alloys. Metall. Mater. Trans. A, 2008, 39: 2435–2448.
[11] Riestra M, Ghassemali E, Bogdanoff T, et al. Interactive effects of grain refinement, eutectic modification and solidification rate on tensile properties of Al-10Si alloy. Materials Science and Engineering: A, 2017, 703: 270–279.
[12] Wu Y, Liu X, Bian X. Effect of boron on the microstructure of near-eutectic Al-Si alloys. Materials Characterization, 2007, 58: 205–209.
[13] Lu S, Hellawell A. The mechanism of silicon modification in aluminum-silicon alloys: Impurity induced twinning. Metallurgical Transactions A, 1987, 18: 1721–1733.
[14] Nogita K, Drennan J, Dahle A. Evaluation of Silicon Twinning in Hypo-Eutectic Al-Si Alloys. Materials Transactions, 2003, 44: 625–628.
[15] Li J H, Albu M, Hofer F, et al. Solute adsorption and entrapment during eutectic Si growth in Al-Sibased alloys. Acta Materialia, 2015, 83: 187–202.
[16] Timpel M, Wanderka N, Schlesiger R, et al. The role of strontium in modifying aluminium-silicon alloys. Acta Materialia, 2012, 60: 3920–3928.
[17] SreejaKumari S S, Pillai R M, Rajan T P D, et al. Effects of individual and combined additions of Be, Mn, Ca and Sr on the solidification behaviour, structure and mechanical properties of Al-7Si-0.3Mg-0.8Fe alloy. Mater. Sci. Eng. A, 2007, 460–461: 561–573.
[18] Zaldívar-Cadena A A, Flores-Valdés A. Prediction and identification of calcium-rich phases in Al-Si alloys by electron backscatter diffraction EBSD/SEM. Materials Characterization, 2007 58: 834–841.
[19] Ludwig T H, Schonhovd D E, Schaffer P L, et al. The effect of Ca and P interaction on the Al-Si eutectic in a hypoeutectic Al-Si alloy. Journal of Alloys and Compounds, 2014, 586: 180–190.
[20] Ceschini L, Morri A, Morri A, et al. Correlation between ultimate tensile strength and solidification microstructure for the sand cast A357 aluminium alloy. Mater. Des., 2009, 30: 4525–4531.
[21] Kavoosi V, Abbasi S M, Mirsaed S M G, et al. Influence of cooling rate on the solidification behavior and microstructure of IN738LC superalloy. Journal of Alloys and Compounds, 2016, 680: 291–300.
[22] Tao R, Zhao Y, Kai X, et al. The effects of Er addition on the microstructure and properties of an in situ nano ZrB2-reinforced A356.2 composite. Journal of Alloys and Compounds, 2018, 731: 200–209.
[23] Jiang W, Fan Z, Liu D, et al. Correlation of microstructure with mechanical properties and fracture behavior of A356-T6 aluminum alloy fabricated by expendable pattern shell casting with vacuum and low-pressure, gravity casting and lost foam casting. Mater. Sci. Eng. A, 2013, 560: 396–403.
[24] Xu C, Xiao W, Hanada S, et al. The effect of scandium addition on microstructure and mechanical properties of Al-Si-Mg alloy: A multi-refinement modifier. Materials Characterization, 2015, 110: 160–169.
[25] Li J, Zhang M, Zhou Y, et al. First-principles study of Al/A1$_3$Ti heterogeneous nucleation interface. Applied Surface Science, 2014, 307: 593–600.
[26] Nayak S S, Pabi S K, Murty B S. Al-(L12)Al$_3$Ti nanocomposites prepared by mechanical alloying: Synthesis and mechanical properties. Journal of Alloys and Compounds, 2010, 492: 128–133.
[27] Gupta R, Chaudhari G P, Daniel B S S. Strengthening mechanisms in ultrasonically processed aluminium matrix composite with in-situ Al$_3$Ti by salt addition. Composites, Part B - Engineering, 2018, 140: 27–34.
[28] Wang S J, Liu G, Wang J, et al. Characteristic orientation relationships in nanoscale Al-Al$_2$Cu Eutectic. Materials Characterization, 2018, 142: 170–178.
[29] Cantor B, Chadwick G A. Crystallography of Al-Al3Ni, Al-Al2Cu and Al-ζ(AlAg) eutectics during nucleation and the early stages of growth. Journal of Crystal Growth, 1975, 30: 101–108.
[30] Wang J, Guo Z, Jiao X Y, et al. On the formation mechanism of the ring-like microstructure of high-pressure die-cast A390 alloy. Materials Characterization, 2018, 140: 179–188.
[31] Wang J, Guo Z, Song J L, et al. On the growth mechanism of the primary silicon particle in a hypereutectic Al-20wt.%Si alloy using synchrotron X-ray tomography. Mater. Des., 2018, 137: 176–183.

This study was financially supported by the National Natural Science Foundation of China (Grant No.51775297), the National Science and the Tsinghua University Initiative Scientific Research Program (20151080370) and the UK Royal Academy of Engineering/Royal Society through the Newton International Fellowship Scheme.